Physics and Imaging in Radiation Oncology 6 (2018) 53–60

Contents lists available at ScienceDirect

Physics and Imaging in Radiation Oncology

journal homepage: www.elsevier.com/locate/phro

Original Research Article

Investigating the role of functional imaging in the management of soft-tissue sarcomas of the extremities

Martin Vallières[a,*], Monica Serban[a], Ibtissam Benzyane[a], Zaki Ahmed[a], Shu Xing[a], Issam El Naqa[b], Ives R. Levesque[a,c], Jan Seuntjens[a,c], Carolyn R. Freeman[c,d]

[a] Medical Physics Unit, McGill University, Cedars Cancer Centre, McGill University Health Centre – Glen Site, 1001 boulevard Décarie, Montréal, QC H4A 3J1, Canada
[b] Department of Radiation Oncology, Physics Division, University of Michigan, 519 W. Williman St. Argus Bldg, Ann Arbor, MI 48103-4943, USA
[c] Research Institute of the McGill University Health Centre, 1001 boulevard Décarie, Montréal, QC H4A 3J1, Canada
[d] Department of Radiation Oncology, Cedars Cancer Centre, McGill University Health Centre – Glen Site, 1001 boulevard Décarie, Montréal, QC H4A 3J1, Canada

ARTICLE INFO

Keywords:
Soft-tissue sarcoma
FDG-PET
FMISO-PET
DW-MRI
DCE-MRI
Texture analysis
Dose painting

ABSTRACT

Background and purpose: In this work, we validate a texture-based model computed from positron emission tomography (PET) and magnetic resonance imaging (MRI) for the prediction of lung metastases in soft-tissue sarcomas (STS). We explore functional imaging at different treatment time points and evaluate the feasibility of radiotherapy dose painting as a potential treatment strategy for patients with higher metastatic risk.

Materials and methods: We acquired fluorodeoxyglucose (FDG)-PET, fluoromisonidazole (FMISO)-PET, diffusion weighting (DW)-MRI and dynamic contrast enhanced (DCE)-MRI data for 18 patients with extremity STS before, during, and after pre-operative radiotherapy. We tested the lung metastases prediction model using pre-treatment images. We evaluated the feasibility of dose painting using volumetric arc therapy (VMAT) via treatment re-planning with a prescription of 50 Gy to the planning target volume (PTV_{50Gy}) and boost doses of 60 Gy to the FDG hypermetabolic gross tumour volume (GTV_{60Gy}) and 65 Gy to the low-perfusion DCE-MRI hypoxic GTV contained within the GTV_{60Gy} (GTV_{65Gy}).

Results: The texture-based model for lung metastases prediction reached an area under the curve (AUC), sensitivity, specificity and accuracy of 0.71, 0.75, 0.85 and 0.82, respectively. Dose painting resulted in adequate coverage and homogeneity in the re-planned treatments: $D_{95\%}$ to the PTV_{50Gy}, GTV_{60Gy} and GTV_{65Gy} were 50.0 Gy, 60.3 Gy and 65.4 Gy, respectively.

Conclusions: Textural biomarkers extracted from FDG-PET and MRI could be useful to identify STS patients that might benefit from dose escalation. The feasibility of treatment planning with double boost levels to intratumoural GTV functional sub-volumes was established.

1. Introduction

Soft-tissue sarcomas (STS) comprise a heterogeneous group of tumours arising from mesenchymal tissues. Standard-of-care treatment consists of surgery combined in many cases with radiotherapy. Pre-operative radiotherapy is now generally favored for the treatment of STS because of the smaller treated volume and lower dose that results in better long-term function as compared with postoperative radiotherapy [1,2]. With such treatment, local control is over 85%. However, about 50% of patients with high grade tumours will develop metastatic disease [3], with the lungs being the main site of metastases (≃80% of cases) [4]. The prognosis of patients who develop lung metastases is poor with a 3-year survival rate of approximately 50% [5]. To date, additional treatment such as chemotherapy has not been shown to prevent the development of metastases or improve survival.

High grade STS are often very large and heterogeneous, often with areas of necrosis. Our hypothesis is that a higher radiotherapy dose given preoperatively to radioresistant/hypoxic components of the tumour could be an effective strategy to improve the outcome for patients at high risk of metastatic disease. Greater tumour cell killing from higher radiotherapy doses would reduce the risk of dissemination of viable tumour cells at surgery as well as the risk of persistent intratumoural hypoxia that can drive the metastatic phenotype [6,7].

Several studies have demonstrated that positron emission tomography (PET) could be used in STS for evaluating prognosis, staging the disease and assessing response to therapy [8–10]. Some studies also observed that glucose demands in hypoxic portions of large tumours may be significantly higher than in normoxic cancer cells [11] and that

* Corresponding author.
E-mail address: mart.vallieres@gmail.com (M. Vallières).

https://doi.org/10.1016/j.phro.2018.05.003
Received 14 October 2017; Received in revised form 6 April 2018; Accepted 8 May 2018

the degree of fluorodeoxyglucose (FDG) uptake may indirectly reflect the level of hypoxia [12]. Evidence in this regard is however not clearly established and the most widely used tracer for non-invasive assessment of hypoxia in solid tumours remains fluoromisonidazole (FMISO). Overall, both FDG-PET and FMISO-PET functional characteristics could be of interest in STS treatment management to identify potential radioresistant regions [13].

The imaging modality of choice for STS is, however, magnetic resonance imaging (MRI) [14–16]. Diffusion-weighted magnetic resonance imaging (DW-MRI) can provide information about cellular density, and dynamic contrast-enhanced magnetic resonance imaging (DCE-MRI) about vascular characteristics [17]. In STS, an increase in apparent diffusion coefficients (ADC) obtained from DW-MRI scans is positively correlated with response to therapy [18] and with a decrease in tumour cellularity [19]. Furthermore, it has been suggested that low-perfusion DCE-MRI information could be used as a surrogate of hypoxia [20,21], and that heterogeneity in DCE-MRI pharmacokinetic maps holds potential as imaging biomarkers of STS response to therapy [22,23].

Tumours exhibiting higher intratumoural heterogeneity are associated with worse prognosis [24–26]. Recently, a model quantifying the heterogeneity of STS tumour sub-regions in terms of size and intensity variations from textural characteristics of fused FDG-PET/MRI pre-treatment images was proposed [27]. This model was developed to assess the likelihood of future development of lung metastases in STS. This information could be useful to identify patients that would benefit the most from dose escalation to hypermetabolic and hypoxic tumour sub-volumes.

In this work, we provide a description of the results derived from a prospective study carried out at our institution. FDG-PET, FMISO-PET, DW-MRI and DCE-MRI data for extremity STS patients were acquired before, during, and after pre-operative radiotherapy (RT). Our main objectives were: i) to validate the texture-based model previously developed for the prediction of lung metastases; ii) to evaluate the complementarity and evolution of PET and MRI functional information over the course of radiotherapy; and iii) to evaluate the feasibility of radiotherapy planning with dose escalation to sub-regions of the gross tumour volume (GTV). We hypothesize that the integration of these three processes into STS management could lead to a novel treatment strategy for patients at higher risk of developing metastatic disease, for which at this time other options (e.g., systemic chemotherapy) are limited.

2. Material and methods

2.1. Patients

Eligible patients were those with age ≥18 years with histologically confirmed primary STS of the extremities without lymph node or distant metastases at presentation and who were deemed suitable for limb preservation surgery. Patients with rhabdomyosarcoma, Ewing sarcoma, osteosarcoma or Kaposi sarcoma, or those with contraindications for MRI (e.g., MRI unsafe because of metallic foreign body in the brain or eye, cochlear implant, some types of pacemakers etc.) were not eligible. The study was approved by the Research Ethics Board of our institution and all patients provided signed informed consent prior to study entry.

Clinical characteristics of the 18 patients accrued to the study between 2013 and 2016 are given in Supplementary Table 2. There were ten males and eight females with a median age of 57.5 years (range: 27–80 years). Nine of the 18 patients had tumours in the thigh, four in the shoulder girdle, three in the arm, and two in the leg. Eleven tumours were > 10 cm in size, six were 5–10 cm, and one was < 5 cm. Thirteen of the 18 patients had high-grade tumours. One patient developed local recurrence, and this patient and six others developed metastatic disease (lung: 5, lymph nodes: 2, bone: 3, liver: 1, soft tissue: 1, adrenal: 1). Four patients have died including two of disease. Twelve patients remained free of disease at a median follow-up of 24 months (range 13–35 months). The median follow-up of the whole cohort was 22 months (range 10–37 months).

2.2. Standard-of-care radiotherapy planning and treatment delivery

Image-guided intensity modulated radiotherapy was applied per our standard practice for all patients. The GTV was delineated on the MRI co-registered to the planning computed tomography (CT) scan. The clinical target volume (CTV) margin was +3 cm proximal and distal and +1.5 cm radially, anatomically confined, i.e., not extending into bone or beyond an intact facial barrier or the skin surface. The planning target volume (PTV) margin was +5 mm, cropped at 5 mm from the skin. Dose prescription was as follows: minimum 50 Gy in 25 fractions to cover 95% of the PTV, > 99% of the PTV to receive > 97% of the prescribed dose, and < 2% of the PTV to receive > 110% of the prescribed dose.

2.3. Study design

FDG-PET, FMISO-PET, DW-MRI and DCE-MRI images were to be collected at pre-radiotherapy (pre-RT), mid-radiotherapy (mid-RT) and post-radiotherapy (post-RT) time points (see details in Supplementary Fig. 1). Image acquisition, interpretation, and registration protocols are given in the Supplementary Material. Standard-of-care MRI data acquired for anatomical tumour definition were also collected including T1-weighted (T1), T2-weighted fat-saturated (T2FS) and T1-weighted post-injection of a gadolinium contrast agent (T1 post-gado) images. We planned a maximum accrual of 20 patients in order to comply with the allowed timeframe of the study protocol, with the expectation that at least 15 patients would complete all required imaging studies as planned.

Overall, complete imaging data comprising FDG-PET, FMISO-PET, DW-MRI and DCE-MRI were obtained at pre-RT for only 14 of the 18 patients. This was due to technical issues with DW-MRI in three patients, and with FMISO-PET in one of these and one additional patient. Only 7 of the 18 patients completed all planned imaging studies, mainly due to patient-related factors (practical difficulties with scheduling, claustrophobia and refusal for other reasons).

2.4. Image analysis

We applied the prediction model fully developed and described in previous work [27] to the new patient cohort of this study. This model linearly combines four texture features extracted from fused FDG-PET/MRI scans: i) small zone emphasis on FDG-PET/T2FS; ii) zone size variance on FDG-PET/T1; iii) high gray-level zone emphasis on FDG-PET/T1; and iv) high gray-level run emphasis on FDG-PET/T2FS. The performance of the complete multivariable model response (defined by the linear coefficients of the model as previously determined in [27]) for predicting the future development of lung metastases in the new cohort of this study was assessed using receiver-operating characteristic (ROC) curve metrics.

FDG-PET and FMISO-PET data were converted into standard uptake value (SUV) maps using injected tracer dose and patient body weight. Apparent diffusion coefficient (ADC) maps were calculated from three DW-MRI series acquired with *b*-values of 100, 500 and 800 s/mm^2, assuming a standard mono-exponential signal decay model and using a linear fit to the natural logarithm of the pixel data. DCE-MRI data were processed using the Tofts model [28] with a population-based model for the arterial input function [29] to produce maps of the permeability constant K^{Trans}. Maps of the initial area under the signal enhancement curve (IAUC) from the injection to 60 s post-injection were also extracted from the DCE-MRI data [30].

Descriptive statistics were first extracted for each tumour at all

available time-points: i) the 75th percentile intensity in FDG-PET and FMISO-PET as a measure of higher metabolism and hypoxia, respectively (units: SUV); ii) the 25th percentile intensity in ADC maps as a measure of low water diffusion in more aggressive tumours [31–32] (units: mm^2/s); and iii) the mean K^{Trans} in DCE-MRI as a global measure of perfusion in the tumour (units: min^{-1}). Note that all metrics were extracted from quantitative parametric maps with units translating to meaningful physical interpretation.

Thresholds of the percentage of maximum intensity on imaging scans were also manually defined to create discrete high-intensity sub-region contours for each patient. For FDG-PET, FMISO-PET, ADC maps from DW-MRI and IAUC maps from DCE-MRI, the average thresholds used were (44 ± 8)%, (45 ± 7)%, (47 ± 7)% and (38 ± 8)%, respectively. For this part of the experiments, IAUC maps were chosen over K^{Trans} maps in DCE-MRI due to the lower tendency of IAUC to generate outlier intensity noise. All images were then brought to a common space (MRI) using rigid registration. To analyze the overlap or complementarity of high intensities on the different pre-RT imaging studies, Dice coefficients [33] were calculated between the high-intensity tumour sub-region masks of the different imaging modalities. For longitudinal analysis, high-intensity tumour sub-region contours were created for the mid-RT and post-RT time points using the same thresholds and methods as for the pre-RT time point. The percentage volume of high-intensity tumour sub-regions relative to the whole tumour volume was calculated for each imaging modality and for each time point. More details about these methods can be found in the Supplementary material.

2.5. Dose painting feasibility study

We evaluated the feasibility of dose painting by re-planning the radiotherapy treatments with dual dose boosts within the GTV (which was originally delineated on MRI for the standard treatment delivered to all patients). First, T1 post-gado, T2FS, DCE-MRI, and FDG-PET/CT were registered to the planning CT scan. The *anatomical* MRI GTV was contoured on a T1 post-gado and/or T2FS axial MRI. In addition, we defined a *metabolic* FDG GTV and a *hypoxic* low perfusion DCE-MRI GTV using threshold percentages of maximum values of SUV maps (30%) and low-perfusion DCE-MRI maps [21] (50%), respectively. The cumulative margin on the MRI GTV for CTV and PTV expansion (PTV_{50Gy}) was planned to receive the standard prescription dose of $D_{95\%}$ = 50 Gy with a maximum dose of 53.5 Gy. The MRI GTV ($GTV_{53.5Gy}$) was prescribed to a dose of $D_{95\%} \geq 53.5$ Gy. The FDG GTV and low-perfusion DCE-MRI GTV sub-volumes within the MRI $GTV_{53.5Gy}$ were planned for dose boosting as follows: i) the FDG GTV (GTV_{60Gy}) was planned to receive a boost dose of $D_{95\%} \geq 60$ Gy with a maximum dose of 65 Gy; and ii) the low-perfusion DCE-MRI GTV (GTV_{65Gy}) contained within the FDG GTV was planned to receive a boost dose of $D_{95\%} \geq 65$ Gy with a maximum dose of 70 Gy. An Eclipse software (V11.0) was used in the re-planning process. Volumetric arc therapy (VMAT) consisting of three 6 MV arcs was used in the process, where two arcs were designed to cover the entire PTV_{50Gy} and the third to cover the boosted GTV_{60Gy} and GTV_{65Gy} only. Overall, based on the delineated GTV sub-volumes, 14 patients of the cohort were deemed suitable to be re-planned with the two levels of dose boosting (60 Gy and 65 Gy). More details about these methods can be found in the Supplementary material.

3. Results

3.1. Prediction of lung metastases development

The texture-based model performed well when applied to the current patient cohort of this work: the area under the ROC curve (AUC) was 0.71, the sensitivity 0.75, the specificity 0.85 and the accuracy 0.82 (Fig. 1). Development of lung metastases (positive and negative) was correctly predicted for 14 out of 17 patients. Supplementary Fig. 2 shows FDG-PET imaging examples over the three time points of four patients; in two of these the model correctly predicted lung metastases (one positive, one negative) and in two it did not (one positive, one negative). These imaging examples suggest that different tumour sub-regions as defined by the FDG uptake may have considerably influenced the textural characteristics of the prediction model.

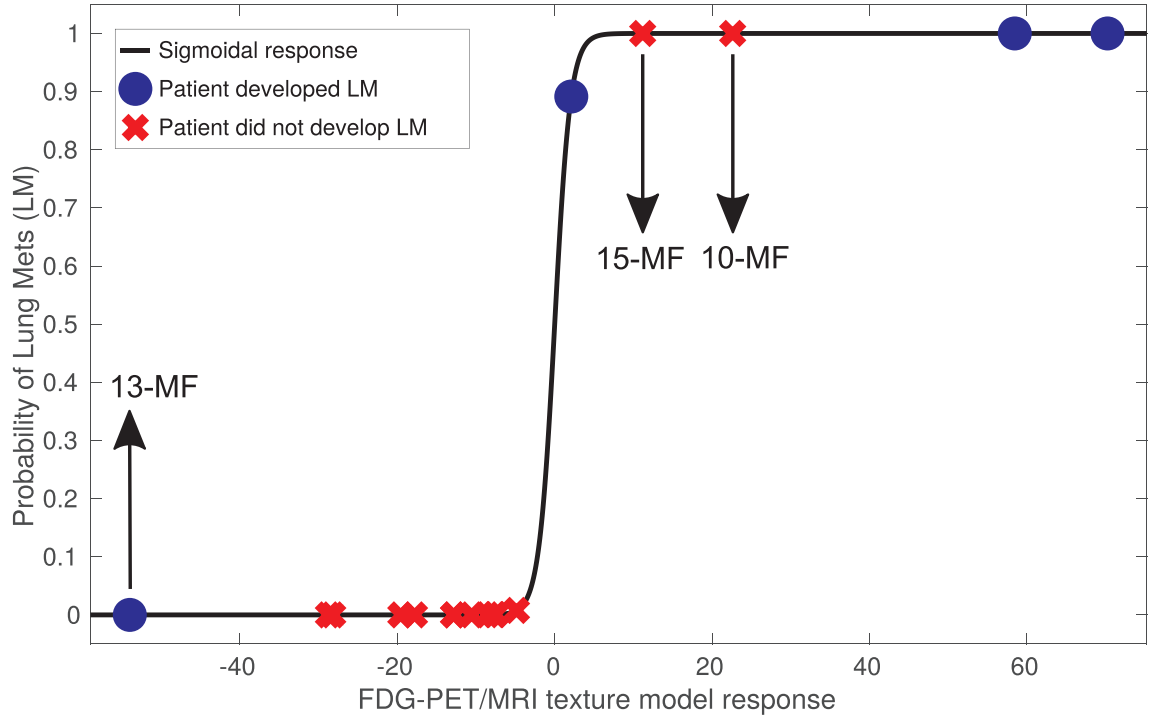

Fig. 1. Response of the FDG-PET/MRI texture-based model developed in previous work on a different retrospective cohort of patients [27], when directly applied on the patient cohort of this study. Abbreviations are defined in Supplementary Table 1.

3.2. General imaging findings

Tumour imaging data generally demonstrated elevated ADC, heterogeneous tumour perfusion elevated in comparison to nearby tissues and elevated FDG uptake. Qualitatively, FMISO-PET images generally provided little supplementary information as compared to FDG-PET. The progression of relevant prognostic imaging metrics for FDG-PET (75^{th} percentile of SUV distribution), FMISO-PET (75^{th} percentile of SUV distribution), DW-MRI (25^{th} percentile of ADC distribution) and DCE-MRI (mean of K^{Trans} distribution) over the course of RT is shown in Fig. 2. The progression of these metrics over the course of RT allowed separation of the patients into three groups (increasing, stable, decreasing). For FDG-PET and FMISO-PET (Fig. 2a and b) the patient groups were largely overlapping, indicating that FMISO-PET provided only modest supplementary information as compared to FDG-PET. In contrast, the patient groups for ADC (Fig. 2c) and K^{Trans} (Fig. 2d) were considerably different than the patient groups observed on PET imaging. Furthermore, the radiation response for patients of the same STS subtype (e.g., myxofibrosarcoma) was not always similar (Fig. 2e). Example images are shown for FDG-PET and FMISO-PET in Supplementary Fig. 2, and for DW-MRI and DCE-MRI in Supplementary Fig. 3. Finally, Spearman correlation analysis (rs) between all pairs of imaging metrics at all RT time points is shown in Supplementary Fig. 4. Significant correlations between different metrics at the same time point were found to be: i) FDG and FMISO at mid-RT ($rs = 0.85$, $p = 0.001$); ii) FDG and FMISO at post-RT ($rs = 0.80$, $p = 0.01$); iii) FDG and ADC at mid-RT ($rs = -0.76$, $p = 0.006$); and iv) ADC and K^{Trans} at pre-RT ($rs = -0.70$, $p = 0.02$).

3.3. Tumour sub-region analysis

High-intensity tumour sub-region contours for the FDG-PET, FMISO-PET, DW-MRI (ADC map) and DCE-MRI (IAUC map) pre-RT scans of an example patient are shown in Fig. 3 (left). Images in Fig. 3a and b suggest that FMISO sub-regions did not bring supplementary information as compared to FDG. On the other hand, as expected, ADC and IAUC sub-regions (Fig. 3c and d) differed considerably from FDG-PET for that patient. Of note, we observed that the FDG-PET high-intensity sub-region seemed to be separated into high- and low-perfusion regions obtained from IAUC maps, the latter indicated by the yellow arrows in Fig. 3d. Using Dice coefficient (s) analysis, we then determined that: i) there was high overlap or low potential of complementarity between high-intensity regions of FDG and FMISO ($s = 0.76 \pm 0.13$); ii) there was medium overlap or medium potential of complementarity between high-intensity regions of FDG and ADC ($s = 0.52 \pm 0.23$), FDG and IAUC ($s = 0.51 \pm 0.15$), FMISO and ADC ($s = 0.58 \pm 0.20$), and FMISO and IAUC ($s = 0.55 \pm 0.15$); and iii) there was low overlap or high potential of complementarity between high-intensity regions of ADC and IAUC ($s = 0.39 \pm 0.17$). In Fig. 3 (right), the box plots show that the percentage of high-intensity sub-regions generally decreased for all imaging studies as RT progressed, except for ADC for which the trend was unclear.

3.4. Evaluation of dose painting feasibility via re-planning of radiotherapy

An example image of low-perfusion DCE-MRI blended with the planning CT of patient 5 is displayed in Fig. 4-left with contours extracted from T1 post-gado ($GTV_{53.5Gy}$), SUV maps (GTV_{60Gy}) and low-perfusion DCE-MRI (GTV_{65Gy}). This image shows that it was possible to define sub-volumes based on functional imaging within the GTV for treatment planning purposes. An example image of the different boost levels of the dose painting distribution on an axial view of the planning CT of patient 5 is displayed in Fig. 4-right. This image shows how the isodose lines of the re-planned treatment closely matched the functional sub-volume delineations of Fig. 4-left. The dose-volume parameters in Table 1 demonstrate that adequate coverage and homogeneity could be achieved within the individual tumour sub-volumes. The $D_{95\%}$ to the PTV_{50Gy}, GTV_{60Gy} and GTV_{65Gy} were 50.0 Gy, 60.3 Gy and 65.4 Gy, respectively. The homogeneity index HI (calculated as the ratio of $D_{5\%}$ to $D_{95\%}$) for the difference volume of GTV_{60Gy} minus GTV_{65Gy}, and for $GTV_{65\ Gy}$, were 1.09 and 1.06, respectively.

4. Discussion

Treatment of soft-tissue sarcomas has become increasingly standardized over the past two decades, with most patients now being treated at diagnosis with a combination of limb-preserving surgery and radiotherapy. While outcomes in terms of local tumour control and function are generally better than in the past, metastatic spread remains an obstacle to cure, particularly for patients with large, high-grade tumours [3]. The prospective study described here was designed to evaluate whether multi-modality imaging could lead to more personalized radiotherapy treatments from the outset by intensifying treatment for patients at greatest risk of metastatic spread. In this work, we described the major results derived from this study and verified the possibility of applying the following strategy for STS treatment management: i) identification of STS patients at higher risk of developing lung metastases via texture analysis of pre-treatment FDG-PET and MRI; ii) delineation of hypermetabolic and hypoxic tumour sub-volumes via functional imaging; and iii) planning radiotherapy delivery with dose escalation to tumour sub-volumes.

First, the texture-based model using FDG-PET and MRI prior to radiotherapy and developed in previous work [27] performed well in predicting future development of lung metastases. To the best of our knowledge, this the first validation in the literature of a lung metastases prediction model in STS based on pre-treatment medical imaging. The information obtained from this model could be useful to identify patients that would potentially benefit the most from dose escalation to different sub-volumes within the GTV. As an example application in the context of the patient population of this study, five patients would have been identified as being at a higher risk of developing lung metastases prior to treatment. Three of the five patients eventually developed lung metastases after having received standard radiotherapy and might potentially have benefited from dose escalation. However, the two patients who did not develop lung metastases (after a median follow-up of 22 months) would also have received extra dose, perhaps unnecessarily, which highlights the need to further improve the specificity of the prediction model.

Changes in anatomical and functional imaging data over the course of radiotherapy were also analyzed. FMISO uptake within the tumours was overall not substantially different from the FDG uptake and generally on the same level as the FMISO uptake within muscles. FDG-PET, DW-MRI and DCE-MRI data displayed considerable inter-patient variability over time, indicating potential for treatment adaptation and personalization. However, progression of simple prognostic metrics from pre- to mid- to post-RT was not consistent between the different imaging modalities. Overall, no clear patient grouping using a single or combination of imaging modalities could be defined for this patient cohort. This attests to the complexity of STS treatment response management and future work with a larger and more homogeneous patient population is warranted to better establish how combinations of functional imaging modalities could be useful to monitor treatment response in STS. In future work, we will also investigate how more complex metrics such as textural biomarkers would change over the course of radiotherapy.

With regards to the evaluation of the feasibility of dose painting via the re-planning of radiotherapy treatments of our patient cohort, our goal had been to achieve an initial level of dose boost to the hypermetabolic tumour sub-regions as seen on the FDG-PET scans, and a second level boost with higher dose to the hypoxic volume contained within the hypermetabolic tumour sub-regions. Since in our experience FMISO-PET did not prove useful in defining the level of hypoxia in STS

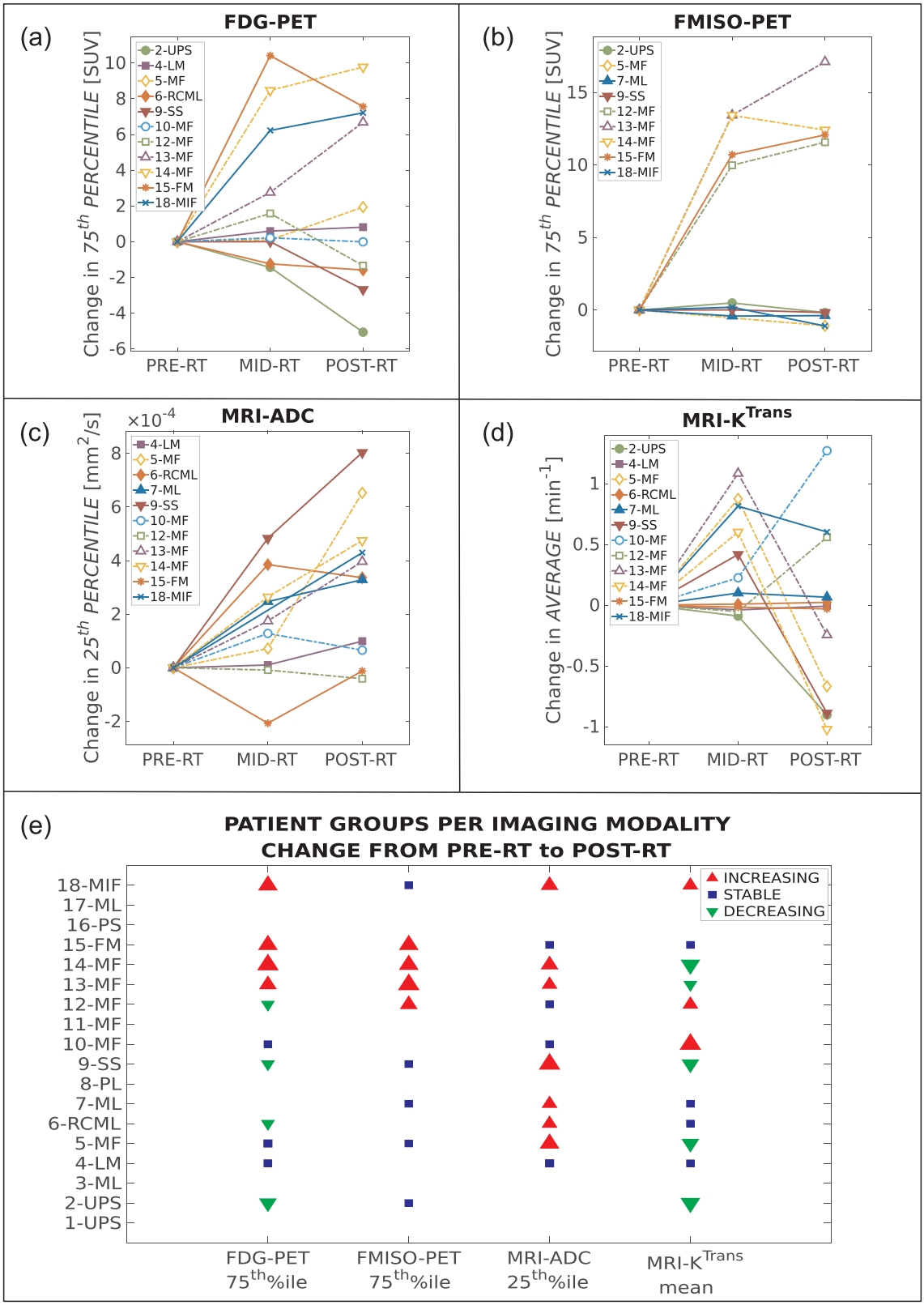

Fig. 2. Changes in relevant prognostic metrics of FDG-PET, FMISO-PET, DW-MRI and DCE-MRI intratumoural data at three time points during radiotherapy (PRE-RT, MID-RT, POST-RT) for patients with available images. (a) 75th percentile of FDG-PET SUV; (b) 75th percentile of FMISO-PET SUV; (c) 25th percentile of ADC maps; (d) Average of K^{Trans} maps; (e) Patient grouping per imaging modality with respect to metric changes from PRE-RT to POST-RT as seen in panels a-b-c-d. The size of the markers is proportional to the absolute change. Abbreviations are defined in Supplementary Table 1.

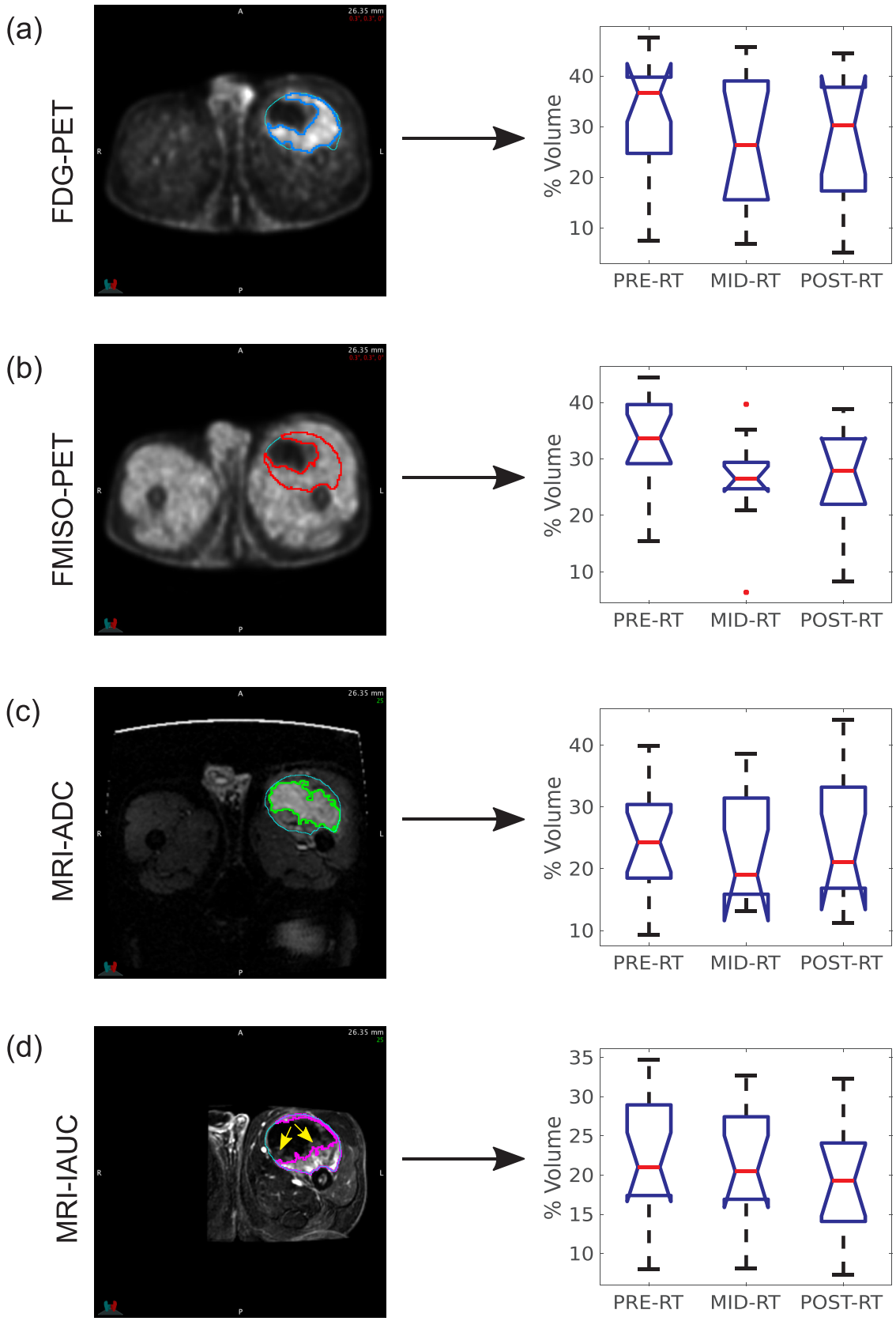

Fig. 3. Analysis of high-intensity tumour sub-regions over time for: (a) FDG-PET scans; (b) FMISO-PET scans; (c) ADC maps; (d) IAUC maps from the injection to 60 s post-injection, with example low perfusion areas identified by yellow arrows. The left column shows example images and high-intensity tumour sub-region contours for the same slice of patient 15 (fibromyxoid sarcoma). The right column summarizes the distribution of volume percentages of high-intensity tumour sub-regions over all patients of the cohort, for the three radiotherapy (RT) treatment time points. Abbreviations are defined in Supplementary Table 1. (For interpretation of the references to colour in this figure legend, the reader is referred to the web version of this article.)

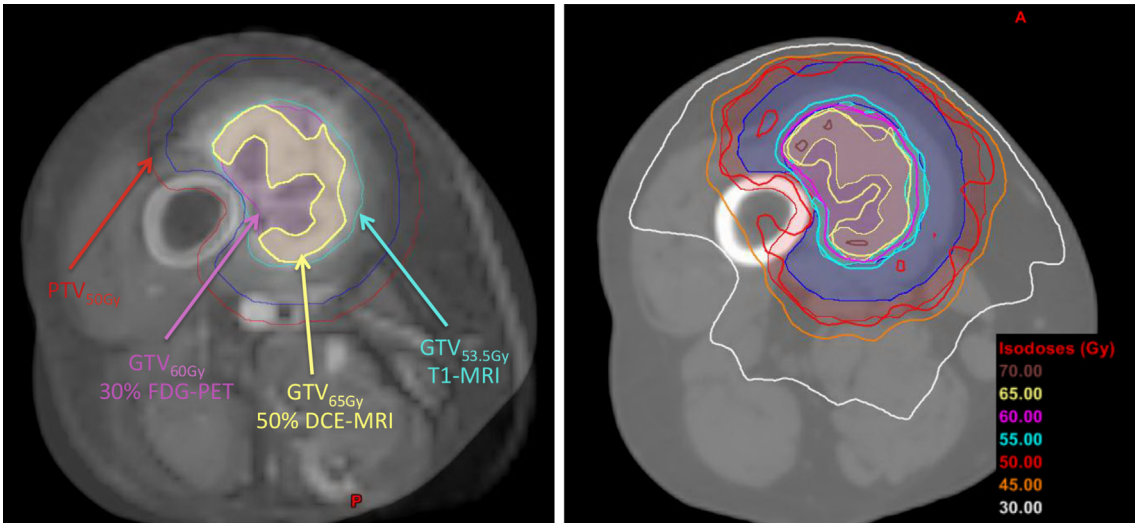

Fig. 4. Dose painting example. Left: Low-perfusion DCE-MRI and CT blended images of patient 5; Right: Dose distribution of patient 5, with different levels of dose boosting. Abbreviations are defined in Supplementary Table 1.

Table 1
Dose-volume parameters (D_x) for the different dose painting boost levels averaged over 14 patients. D_{Mean} is the mean dose in the volume. The homogeneity index (HI) was calculated as the ratio of $D_{5\%}$ to $D_{95\%}$ for the following differential volumes: (i) $PTV_{50Gy} - GTV_{53.5Gy}$; (ii) $GTV_{53.5Gy} - GTV_{60Gy}$; (iii) $GTV_{60Gy} - GTV_{65Gy}$; and (iv) GTV_{65Gy}. Abbreviations are defined in Supplementary Table 1.

Region of interest	$D_{95\%}$ (Gy)	D_{Mean} (Gy)	HI
PTV_{50Gy}	50.0 ± 0.03	52.1 ± 0.5	1.09 ± 0.02 (i)
$GTV_{53.5Gy}$	54.4 ± 2.5	56.7 ± 1.5	1.17 ± 0.03 (ii)
GTV_{60Gy}	60.3 ± 0.2	62.7 ± 0.5	1.09 ± 0.02 (iii)
GTV_{65Gy}	65.4 ± 0.4	67.6 ± 0.3	1.06 ± 0.01 (iv)

as compared to nearby muscles, we used a low-perfusion DCE volume as a surrogate to hypoxia [20,21]. We observed in most patients that high-activity FDG tumour sub-regions (i.e., excluding the inactive or necrotic part of the tumour) could be distinctly separated into high- and low-perfusion sub-volumes. Furthermore, some studies suggested that higher radiotherapy doses could lead to better local control in retroperitoneal sarcomas [34,35] and that a boost dose of 57.5 Gy to the margin at risk could be well-tolerated in STS patients [36]. In contrast, we demonstrated in our study that dose escalation with VMAT boosting to multiple GTV sub-volumes in STS could also be technically feasible: we achieved two levels of dose boost of 60 Gy and 65 Gy within the GTV in the re-planning process of our patient cohort. It is important to note that in this work, re-planning was performed for all suitable patients of our cohort in order to better verify the feasibility of the exercise, in contrast to re-planning only patients identified at higher risk of developing metastases with the texture-based model as it could be performed in a potential clinical scenario. However, the clinical feasibility and benefit of such dose escalation scheme in terms of risk of wound healing complications versus distant metastasis rates needs to be verified. Changes in hypermetabolic and hypoxic sub-regions would also need to be monitored frequently, even daily, during radiotherapy. In this context, DW-MRI and DCE-MRI would be preferable to PET, particularly with the advent of novel MR-linac technologies. Notably, future work should investigate how to capture both high metabolism and hypoxia in STS using, for example, DCE-MRI surrogates.

Overall, this work represented a unique experience for the investigation of multi-modality imaging characteristics over the course of treatment of STS and raised the possibility of a new strategy for managing patients at high risk of metastatic spread. However, there were several caveats. First, our cohort was small and heterogeneous with respect to tumour location, size and pathological type. Secondly, uncertainties in PET and MR image registration may have impacted the analysis of the complementarity of tumour sub-regions defined from different imaging modalities. Also, in our experience, we found that it was not feasible to acquire three imaging scans (FDG-PET, FMISO-PET, MRI) at three different time points of radiotherapy (pre-RT, mid-RT, post-RT), primarily for practical reasons (mostly patient acceptance). Simplification of image acquisition is planned in future studies. Finally, investigating the correlation of surgical outcomes (e.g., R-stage, pathologic findings, etc.) with functional imaging will be important in future prospective studies to better understand the role of multi-modality imaging in the management of STS.

In conclusion, FDG-PET and MRI texture features as routinely obtained in our centre prior to radiotherapy may be useful to predict development of lung metastases in STS and to identify patients that could benefit from dose escalation. Despite the complexity of the multiple targets, dose escalation with two levels of dose boost within the planning GTV using a combination of FDG-PET and DCE-MRI seems technically feasible. Larger STS cohorts are required to validate these findings in future prospective studies.

Conflict of interest

None.

Acknowledgments

This work was supported by the Canadian Institutes of Health Research (CIHR) under grants MOP-114910 and MOP-136774. We would like to thank Asha K. Jeyaseelan and Seema Ambereen for help with patient recruitment and study management, Dr. Lara Hathout for help in writing the initial proposal, Ralf Schirrmacher for supplying the FDG and FMISO, and Drs. Marc Hickeson, Tom Powell and Robert Turcotte for providing expert knowledge. Special thanks to all the PET and MRI technicians for making this study possible.

Appendix A. Supplementary data

Supplementary data associated with this article can be found, in the online version, at http://dx.doi.org/10.1016/j.phro.2018.05.003.

References

[1] O'Sullivan B, Davis AM, Turcotte R, Bell R, Catton C, Chabot P, et al. Preoperative versus postoperative radiotherapy in soft-tissue sarcoma of the limbs: a randomised trial. Lancet 2002;359:2235–41.

[2] Davis AM, O'Sullivan B, Turcotte R, Bell R, Catton C, Chabot P, et al. Late radiation morbidity following randomization to preoperative versus postoperative radiotherapy in extremity soft tissue sarcoma. Radiother Oncol 2005;75:48–53.

[3] Brennan MF. Soft tissue sarcoma: advances in understanding and management. The Surgeon 2005;3:216–23.

[4] Lewis JJ, Brennan MF. Soft tissue sarcomas. Curr Probl Surg 1996;33:839–72.

[5] Billingsley KG, Burt ME, Jara E, Ginsberg RJ, Woodruff JM, Leung DH, et al. Pulmonary metastases from soft tissue sarcoma. Ann Surg 1999;229:602–12.

[6] Bristow RG, Hill RP. Hypoxia and metabolism. Hypoxia, DNA repair and genetic instability. Nat Rev Cancer 2008;8:180–92.

[7] Wouters BG, Koritzinsky M. Hypoxia signalling through mTOR and the unfolded protein response in cancer. Nat Rev Cancer 2008;8:851–64.

[8] Schwarzbach MHM, Hinz U, Dimitrakopoulou-Strauss A, Willeke F, Cardona S, Mechtersheimer G, et al. Prognostic significance of preoperative [18-F] fluorodeoxyglucose (FDG) positron emission tomography (PET) imaging in patients with resectable soft tissue sarcomas. Ann Surg 2005;241:286–94.

[9] Toner GC, Hicks RJ. PET for sarcomas other than gastrointestinal stromal tumors. Oncologist 2008;13:22–6.

[10] Skamene SR, Rakheja R, Dalhstrom KR, Roberge D, Nahal A, Charest M, et al. Metabolic activity measured on PET/CT correlates with clinical outcomes in patients with limb and girdle sarcomas. J Surg Oncol 2014;109:410–4.

[11] Li XF, Du Y, Ma Y, Postel GC, Civelek AC. 18F-Fluorodeoxyglucose uptake and tumor hypoxia: revisit 18F-Fluorodeoxyglucose in oncology application. Transl Oncol 2014;7:240–7.

[12] Dierckx RA, Van de Wiele C. FDG uptake, a surrogate of tumour hypoxia? Eur J Nucl Med Mol Imaging 2008;35:1544–9.

[13] Rajendran JG, Wilson DC, Conrad EU, Peterson LM, Bruckner JD, Rasey JS, et al. [18F]FMISO and [18F]FDG PET imaging in soft tissue sarcomas: correlation of hypoxia, metabolism and VEGF expression. Eur J Nucl Med Mol Imaging 2003;30:695–704.

[14] Bland KI, McCoy DM, Kinard RE, Copeland EM. Application of magnetic resonance imaging and computerized tomography as an adjunct to the surgical management of soft tissue sarcomas. Ann Surg 1987;205:473–81.

[15] Aga P, Singh R, Parihar A, Parashari U. Imaging spectrum in soft tissue sarcomas. Indian J Surg Oncol 2011;2:271–9.

[16] Raghavan M. Conventional modalities and novel, emerging imaging techniques for musculoskeletal tumors. Cancer Control 2017;24:161–71.

[17] Fayad LM, Jacobs MA, Wang X, Carrino JA, Bluemke DA. Musculoskeletal tumors: how to use anatomic, functional, and metabolic MR techniques. Radiology 2012;265:340–56.

[18] Einarsdóttir H, Karlsson M, Wejde J, Bauer HCF. Diffusion-weighted MRI of soft tissue tumours. Eur Radiol 2004;14:959–63.

[19] Schnapauff D, Zeile M, Niederhagen MB, Fleige B, Tunn PU, Hamm B, et al. Diffusion-weighted echo-planar magnetic resonance imaging for the assessment of tumor cellularity in patients with soft-tissue sarcomas. J Magn Reson Imaging 2009;29:1355–9.

[20] Cho H, Ackerstaff E, Carlin S, Lupu ME, Wang Y, Rizwan A, et al. Noninvasive multimodality imaging of the tumor microenvironment: registered dynamic magnetic resonance imaging and positron emission tomography studies of a preclinical tumor model of tumor hypoxia. Neoplasia 2009;11:247–59.

[21] Stoyanova R, Huang K, Sandler K, Cho H, Carlin S, Zanzonico PB, et al. Mapping tumor hypoxia in vivo using pattern recognition of dynamic contrast-enhanced MRI data. Transl Oncol 2012;5:437–47.

[22] van Rijswijk CSP, Geirnaerdt MJA, Hogendoorn PCW, Peterse JL, van Coevorden F, Taminiau AHM, et al. Dynamic contrast-enhanced MR imaging in monitoring response to isolated limb perfusion in high-grade soft tissue sarcoma: initial results. Eur Radiol 2003;13:1849–58.

[23] Alic L, van Vliet M, van Dijke CF, Eggermont AMM, Veenland JF, Niessen WJ. Heterogeneity in DCE-MRI parametric maps: a biomarker for treatment response? Phys Med Biol 2011;56:1601–16.

[24] Fidler IJ. Critical factors in the biology of human cancer metastasis: twenty-eighth G.H.A. Clowes memorial award lecture. Cancer Res 1990;50:6130–8.

[25] Yokota J. Tumor progression and metastasis. Carcinogenesis 2000;21:497–503.

[26] Campbell PJ, Yachida S, Mudie LJ, Stephens PJ, Pleasance ED, Stebbings LA, et al. The patterns and dynamics of genomic instability in metastatic pancreatic cancer. Nature 2010;467:1109–13.

[27] Vallières M, Freeman CR, Skamene SR, El Naqa I. A radiomics model from joint FDG-PET and MRI texture features for the prediction of lung metastases in soft-tissue sarcomas of the extremities. Phys Med Biol 2015;60:5471–96.

[28] Tofts PS, Brix G, Buckley DL, Evelhoch JL, Henderson E, Knopp MV, et al. Estimating kinetic parameters from dynamic contrast-enhanced T(1)-weighted MRI of a diffusible tracer: standardized quantities and symbols. J Magn Reson Imaging 1999;10:223–32.

[29] Parker GJM, Roberts C, Macdonald A, Buonaccorsi GA, Cheung S, Buckley DL, et al. Experimentally-derived functional form for a population-averaged high-temporal-resolution arterial input function for dynamic contrast-enhanced MRI. Magn Reson Med 2006;56:993–1000.

[30] Evelhoch JL. Key factors in the acquisition of contrast kinetic data for oncology. J Magn Reson Imaging 1999;10:254–9.

[31] Oka K, Yakushiji T, Sato H, Hirai T, Yamashita Y, Mizuta H. The value of diffusion-weighted imaging for monitoring the chemotherapeutic response of osteosarcoma: a comparison between average apparent diffusion coefficient and minimum apparent diffusion coefficient. Skeletal Radiol 2010;39:141–6.

[32] Schmeel FC, Simon B, Sabet A, Luetkens JA, Träber F, Schmeel LC, et al. Diffusion-weighted magnetic resonance imaging predicts survival in patients with liver-predominant metastatic colorectal cancer shortly after selective internal radiation therapy. Eur Radiol 2017;27:966–75.

[33] Dice LR. Measures of the amount of ecologic association between species. Ecology 1945;26:297–302.

[34] Fein DA, Corn BW, Lanciano RM, Herbert SH, Hoffman JP, Coia LR. Management of retroperitoneal sarcomas: does dose escalation impact on locoregional control? Int J Radiat Oncol Biol Phys 1995;31:129–34.

[35] Feng M, Murphy J, Griffith KA, Baker LH, Sondak VK, Lucas DR, et al. Long-term outcomes after radiotherapy for retroperitoneal and deep truncal sarcoma. Int J Radiat Oncol Biol Phys 2007;69:103–10.

[36] Tzeng CWD, Fiveash JB, Popple RA, Arnoletti JP, Russo SM, Urist MM, et al. Preoperative radiation therapy with selective dose escalation to the margin at risk for retroperitoneal sarcoma. Cancer 2006;107:371–9.